Vacuum 101 (2014) 337–344

Contents lists available at ScienceDirect

Vacuum

journal homepage: www.elsevier.com/locate/vacuum

Numerical investigation of three turbomolecular pump models in the free molecular flow range

Yanwu Li [a,*], Xuekang Chen [a], Yanhui Jia [b], Mingzheng Liu [b], Zhong Wang [a]

[a] Science and Technology on Surface Engineering Laboratory, Lanzhou Institute of Physics, P.O. Box 94, Lanzhou, Gansu 730000, PR China
[b] Science and Technology on Vacuum and Cryogenics Technology and Physics Laboratory, Lanzhou Institute of Physics, P.O. Box 94, Lanzhou, Gansu 730000, PR China

ARTICLE INFO

Article history:
Received 30 August 2013
Received in revised form
29 September 2013
Accepted 2 October 2013

Keywords:
Turbomolecular pump
2D model
3D model
Monte Carlo method

ABSTRACT

Selecting a suitable model is important for the quick and accurate calculation of the pumping characteristics of a turbomolecular pump (TMP). Three different calculation models (2D, ideal 3D, and real 3D models) in the free molecular flow range were investigated in this study through the Monte Carlo method. Results show that when blade velocity ratio $C \leq 1$, the simple ideal 3D model with paralleled blades is a better substitute for the complicated real 3D model compared with the 2D model. When $C \geq 2$, maximum compression ratio K_{max} of the TMP calculated with the 2D or ideal 3D models tends to saturate as C increases. However, the results computed with the real 3D model increase exponentially as C increases. Further investigation shows that in the rotating reference frame, molecules move toward the tip wall as a result of Coriolis and centrifugal acceleration, resulting in a significantly large K_{max} and perfect pumping speed.

1. Introduction

Turbomolecular pumps (TMPs) provide a clean and powerful vacuum and are widely used in industrial and scientific applications. The mechanisms of TMPs have been studied extensively to optimize blade design. Pumping performance in the free molecular region was first analyzed by Kruger in 1960 [1]. Kruger modeled the single-blade row of a TMP as a 2D array of flat plates moving between two regions, where the molecular velocity spectrum exhibited Maxwellian distribution. Kruger's theoretical and experimental results were in good agreement. Considering that the 2D model is the simplest, it has been used extensively in the integral equation [1–3], discrete direction-element [4], statistical mechanics [5], and Monte Carlo methods [1,4,6–12]. Another simple model is the ideal 3D, wherein the blades are assumed to be parallel to one another and the velocities of the tips and roots of the blades are assumed to be equal. These assumptions in the ideal 3D model simplify the real geometry of TMPs significantly. Versluis et al. [13] utilized this model to perform direct simulation Monte Carlo (DSMC) simulations on TMP in the free molecular and transitional flow regimes. The results of their study were in excellent agreement with the well-known and often cited experimental results of Sawada [3].

Theoretically, the length between the root and the tip of the blades must be significantly larger than the spacing s but considerably smaller than the radius of the blades for the 2D model to be accurate [4]. Meanwhile, for the ideal 3D model to be accurate, the length between the root and the tip of the blades must also be significantly smaller than the radius of the blades, and the angle between two adjacent blades should be almost zero [13]. These assumptions are difficult to meet in an actual TMP. The real 3D model hardly makes any assumptions on the geometry of TMPs and has been used extensively to perform simulations on single-stage [4,11,14–16] or multistage [17–20] TMPs. Several researchers compared their theoretical and experimental results and found consistency between the two.

Although the real 3D model demonstrates the actual geometry of the TMP, the molecular trajectories in the rotating reference frame are not straight, and the algorithm used in this model is complicated because of geometric complexity [4,11,14,15]. Thus, the 2D and ideal 3D models may still prove valuable for blade design in the future. Selecting a suitable model is the key factor to calculating pumping characteristics quickly and accurately. Katsimichas et al. [4] compared the 2D and real 3D models in the free molecular flow range and found that 2D simulation underestimates maximum compression ratio K_{max}. Schneider et al. [11] obtained a similar

* Corresponding author. Tel.: +86 931 4585223; fax: +86 931 8265391.
E-mail address: andersonliyanwu@sina.com (Y. Li).

0042-207X/$ – see front matter © 2013 Elsevier Ltd. All rights reserved.
http://dx.doi.org/10.1016/j.vacuum.2013.10.002

conclusion. However, more detail analysis is still needed. This study aims to determine the differences among the aforementioned three models through both test particle Monte Carlo (TPMC) and DSMC in the free molecular flow region, particularly in cases involving extremely high rotational speeds.

2. Statement of the problem

The assumptions for the numerical investigation of TMPs in the free molecular flow region are as follows [4,11,21]: (1) no intermolecular collisions occur in the TMP passages; (2) both the inlet and outlet sides of the TMP face extremely large spaces, thereby establishing a Maxwellian velocity distribution; (3) gas molecules are diffusely reflected in the collisions with the walls of TMPs according to the cosine law; and (4) the temperature is constant, and the system is steady.

2.1. Three different TMP models

Fig. 1 shows the schemes of the three different TMP models. Blade thickness is ignored. The 2D model shown in Fig. 1(a) is the simplest, having only three parameters; s is the distance between the blades, b is the length of the blades, and α is the angle of the blades. The ideal 3D model shown in Fig. 1(b) is relatively simple. It has an additional parameter, namely, h or the radial distance between the root and tip of the blade. Fig. 1(c) shows the real 3D model; ψ is the angle between the two center lines of blades A and B, and r_{tip} and r_{root} are the radii of the blade tip and blade root, respectively. Two dimensionless groups are necessary to compare the three models. These groups are blade length ratio $S_0 = s/b$ and blade velocity ratio $C = V_b/V_p$, where V_b is blade velocity normalized by the most probable speed of molecules V_p. In the real 3D model, S_0 and C are determined by the root mean squared radii [4,11]

$$r_{m-sq} = \sqrt{\frac{r_{root}^2 + r_{tip}^2}{2}}. \tag{1}$$

s and V_b are provided by

$$\begin{aligned} s &= 2r_{m-sq}\sin(\psi/2) \\ V_b &= 2\pi\omega r_{m-sq} \end{aligned} \tag{2}$$

where ω is the rotational speed of the pump.

S_0 and α are 1.0 and $\pi/6$, respectively, for all models in this study. All dimensionless parameters can then be determined. s and b are 1.0 in the 2D model. In the ideal 3D model, s and b are 1.0 and h/s is 1.267. r_{tip} is 1.0, r_{root} is 0.8, ψ is $\pi/18$, and $(r_{tip} - r_{root})/s$ is 1.267 in the real 3D model.

2.2. Monte Carlo method

In all three models, the numerical problem of the TPMC (or DSMC) method includes two separate procedures: (1) tracking a particle (or a large number of particles) until it is (they are) lost from the calculation domain, and (2) sampling particle histories. Molecules individually enter the passage in the TPMC method. When one particle leaves the calculation domain, another particle is generated and enters the domain. The TPMC method is often used to calculate the molecular flow transmission probabilities through the TMP passages [1,4,11,12,17–20]. The molecules enter in succession in the DSMC method, such that a large number of particles follow simultaneously. The DSMC method was introduced in Bird's monograph [22], it has been widely used to calculate the pumping characteristics of TMPs in the free molecular flow, transitional flow, and even hydrodynamic flow regimes [6–10,13–16]. The uncoupling of the molecular motion and collisions over small time steps and the partitioning of the physical domain into small cells are the key computational assumptions of DSMC. In the present study, intermolecular collisions were neglected (free molecular flow), and the DSMC method was employed to calculate the K_{max} of every stage of the multistage TMP and to record gas density and flow. The number of incident molecules per unit time in both the inlet and outlet of the TMP was determined first using the TPMC method.

The main performance indices of the TMP are maximum compression ratio K_{max} and maximum pumping speed factor W. These indices are obtained as follows:

$$K_{max} = M_{12}/M_{21}, \quad W = M_{12} - M_{21} \tag{3}$$

where M_{12} is the probability of the transmission of the particle from the upstream side to the downstream side and M_{21} is the probability of the transmission of the particle from the downstream side to the upstream side.

The algorithm of the 2D model is simple; some details can be found in Ref. [1]. The ideal 3D model is also simple; its algorithm requires some improvement compared with that of the 2D model. In the 2D and ideal 3D models, the blades move in a linear manner; thus, the trajectories of the particles in the blades' frame of reference are straight. Simulating 1×10^7 particles on a personal

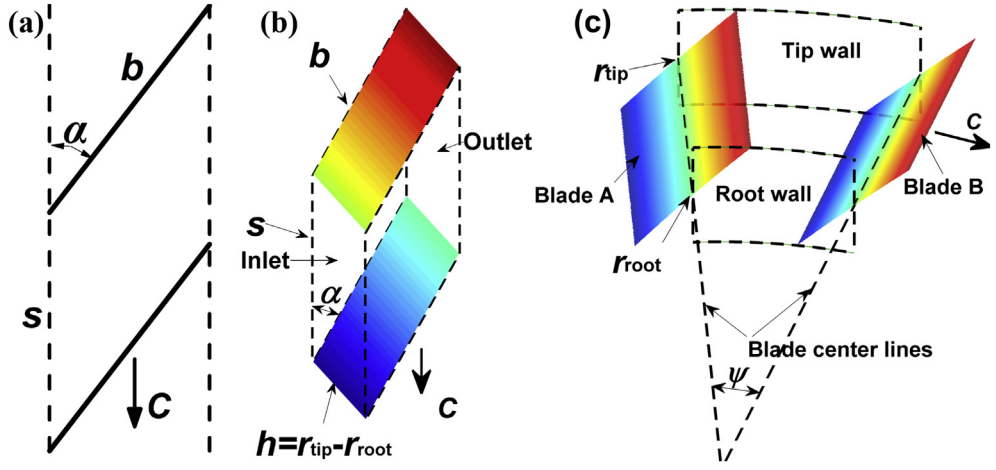

Fig. 1. Schemes of the three different TMP models: (a) 2D model, (b) ideal 3D model, and (c) real 3D model.

computer often requires only a few minutes when these two models are used. By contrast, the algorithm of the real 3D model is much more complex; some details can be found in Refs. [4,14,15,17–19]. In Refs. [14,15], the rotating frame of reference was utilized to simulate a single-stage TMP from free molecular flow to transition flow. Katsimichas et al. in Ref. [4] employed cylindrical coordinates (r, θ, z) for calculation and divided the passage into N_z thin layers with $N_z + 1$ intersections normal to the z axis called z planes for simplicity. Time step dt was obtained to proceed to the next z plane; $dt = dz/v_z$, where dz is the distance between two successive z planes. Amoli, Hosseinalipour, and Ebrahimi in Refs. [17–19] provided very detailed mathematical descriptions of the geometry of the TMP; these mathematical descriptions are the foundation of the algorithm in the present study. After introducing the analytical equations of the blades and molecular trajectories, they calculated the intersection points of the molecular path and blade walls through the bisection method. In the present study, a Fortran program was created based on the method in Refs. [17–19]. To verify this method, another method similar to that of Katsimichas et al. was also used. The calculation domain between two successive blades was divided into $1000 \times 1000 \times 1000$ cells in the other method. The size of the movement step in each time step dt does not exceed that of each cell along r, θ, and z. When the displacement of each step is sufficiently small, the expression of such displacement in Eq. (5) of Ref. [17] could be simplified as follows:

$$\begin{aligned} \mathrm{d}r &= v_r \mathrm{d}t \\ \mathrm{d}\theta &= v_\theta \mathrm{d}t/r \\ \mathrm{d}z &= v_z \mathrm{d}t \end{aligned} \tag{4}$$

where v_r, v_θ, and v_z are the velocity components in the blade's frame of reference. v_r and v_θ should be updated according to Eq. (6) of Ref. [17] at the end of each step. When the total number of simulated particles passing through the TMP is 10^6, the typical error of the Monte Carlo simulation is below 10^{-3} [4]. The relative differences between the values calculated with two different methods in terms of M_{12} (or M_{21}) of a single-stage TMP are below the uncertainties of the Monte Carlo simulation. The real 3D model in this study was solved with the latter method. Furthermore, Weighting factors (WF, which is an integer) were also utilized to obtain M_{21} of multistage TMPs. When a particle comes from an upstream stage of a TMP to the adjacent downstream stage, this particle will be discarded with the probability (WF − 1)/WF. Conversely, if the particle comes from a downstream stage to the adjacent upstream stage, WF − 1 particles with the same velocity and coordinate will be added to the calculation domain. The weighting factors introduced by Bird [22] are widely utilized in rarefied gas dynamics, such as gas flow in tubes [23,24]. Except for the real 3D case, the 2D and ideal 3D programs have also been checked by comparing their results with those in Refs. [1,13].

3. Results and discussions

3.1. Single-stage TMP

The clearances between the blades and the walls of single-stage TMPs were ignored in the 3D models to simplify calculation as shown in Figs. 2-6. Maximum compression ratio K_{max} and maximum pumping speed factor W are plotted versus blade velocity ratio C in Fig. 2. These values were obtained with M_{12} and M_{21} in Eq. (3). The incident molecules were assumed to have stream velocity C relative to the blades to calculate the stator results. No differences were found between the rotor and stator for M_{12} and M_{21} calculated with the 2D or ideal 3D models. Thus, the results of the stator calculated with these two models are not shown in Fig. 2. Fig. 2(a) shows that when $C = 5.0$, the K_{max} of a rotor is 1866 in the real 3D model, 10.06 in the 2D model, and 16.04 in the ideal 3D model. When C increases, the K_{max} of a rotor increases exponentially in the real 3D model but is saturated in the other two models. These results are consistent with those of Katsimichas et al. When $C = 5.0$, the result of the stator is only 14.71 although the K_{max} of a rotor in the real 3D model is as large as 1866; the values calculated with the two 3D models are larger than that calculated with the 2D model. Fig. 2(b) shows W versus C. In a real 3D rotor, W increases to almost 1.0 when C increases. However, W is saturated and reaches its maximum value at $C = 2.5$ in the two other models.

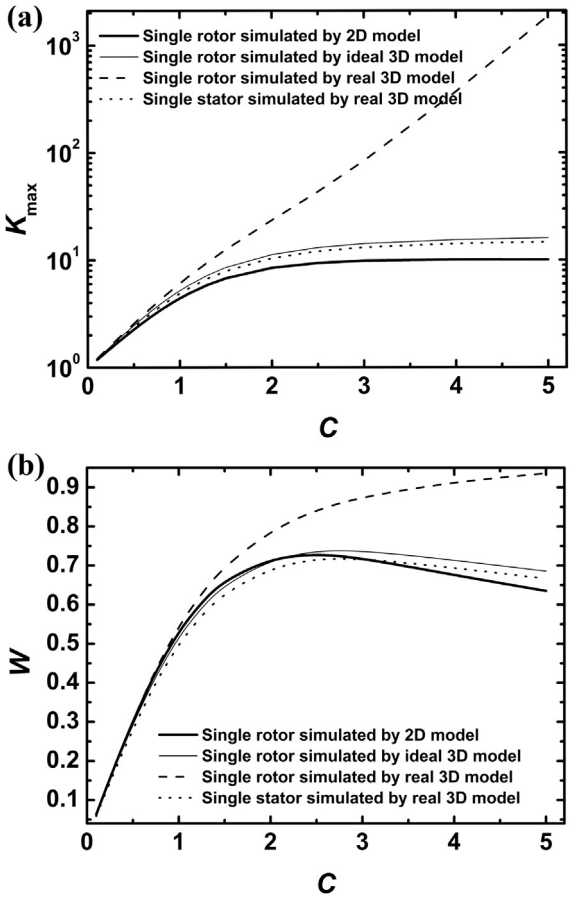

Fig. 2. Pumping performance of the single-stage TMP calculated with the different models and TPMC method: (a) maximum compression ratio K_{max} versus C and (b) maximum pumping speed factor W versus C. The total number of simulated particles is 1×10^7 for each value.

Chu and Hua proved that adding a moving wall enhances K_{max} in the 2D model from the viewpoint of statistical mechanics [5]. Fig. 3 shows the transmission probabilities $M_{12}(r)$ and $M_{21}(r)$ versus the radii of the incident points of the simulated particles at $C = 3.0$. Each rotor has a moving wall near the blade tip (see Fig. 1(c)). $M_{12}(r)$ simulated by the 3D models increases as the radius increases until the radius is almost 1.0. By contrast, $M_{21}(r)$ simulated by the 3D models always decreases as the radius increases. A moving wall is situated near the blade root of each stator, and similar conclusions were obtained. These results indicate that the effect of the moving wall is significant. As shown in Fig. 3(b), M_{21} computed with the two 3D models are significantly lower than that computed with the 2D model, resulting in a larger K_{max}. As seen in Fig. 2(a), the K_{max} of the ideal 3D model is 44.3% larger than that of the 2D model at $C = 3.0$. This result agrees well with the theory of Chu and Hua.

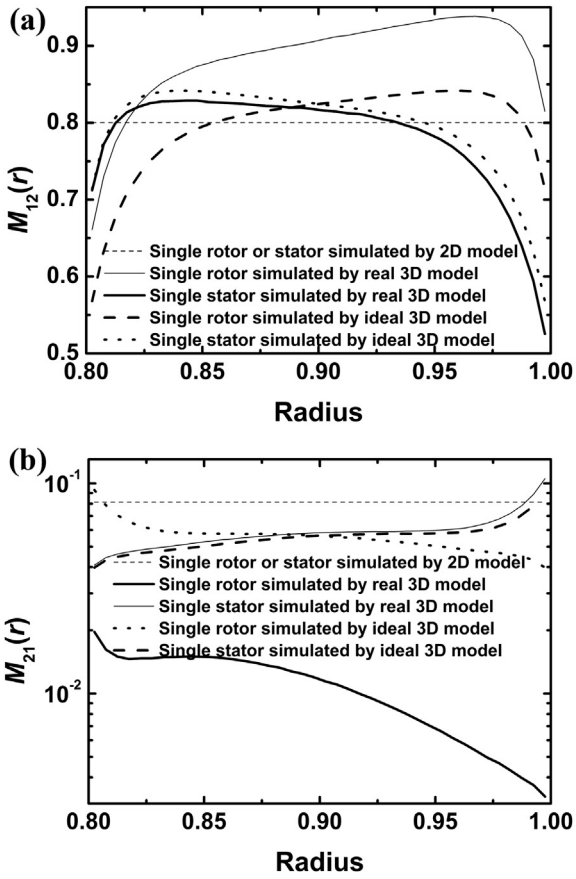

Fig. 3. Transmission probabilities of particles versus the radii of the incident points of the simulated particles at $C = 3.0$. The results are obtained through TPMC method. The total number of simulated particles is 1×10^7 for each value.

The effects of the Coriolis and centrifugal forces [14,15] were also investigated. Figs. 4 and 5 show the probabilities of particles going to a number of surfaces versus blade velocity ratio C in a rotor. The trajectories of simulated particles in the real 3D model were recorded through TPMC method until these trajectories leave the calculation domain. After simulating 10^7 particles, the number of times and the probabilities of particles moving directly to all six surfaces from a particular surface were determined. All simulated particles enter the passage from the outlet in Fig. 4. A particle may come from blade A and then go back to this blade without colliding with other surfaces as shown in Fig. 4(b); the probability of this event occurring is as high as 4.67% when $C = 10.0$. However, such event would never occur in 2D and ideal 3D models. Fig. 4(a)–(c) shows that regardless of where the particles originate, the probabilities of the particles moving to blade B, the root wall, and the inlet decrease rapidly as C increases, whereas the probabilities of particles moving to blade A increase rapidly. When a particle collides with blade B or the root wall of a rotor, then this particle is more likely to reach the inlet and worsen the pumping performance. When a particle collides with blade A, then this particle is more likely to return to the outlet (see Fig. 1(c)).

The simulated particles enter the passage from the inlet in Fig. 5. Regardless of where the particles originate, the probabilities of moving to blade B or the root wall decrease as C increases, whereas the probabilities of particles moving to blade A increase. These results are similar to those shown in Fig. 4. As seen in Fig. 4, when $C = 3.0$ and all the simulated particles enter the passage from the outlet, the probability of particles moving from the outlet to blade A is 94.77%. The probability of particles moving from blade A to the outlet and the tip wall is 76.99% and 19.32%, respectively, and that moving from the tip wall to blade A and the outlet is 82.16% and 17.37%, respectively. As shown in Fig. 5, when $C = 3.0$ and all the simulated particles enter the passage from the inlet, the probabilities of particles moving from the inlet to blade A and the outlet are 60.53% and 24.83%, respectively. The probabilities of particles moving from blade A to the outlet and the tip wall are 46.56% and

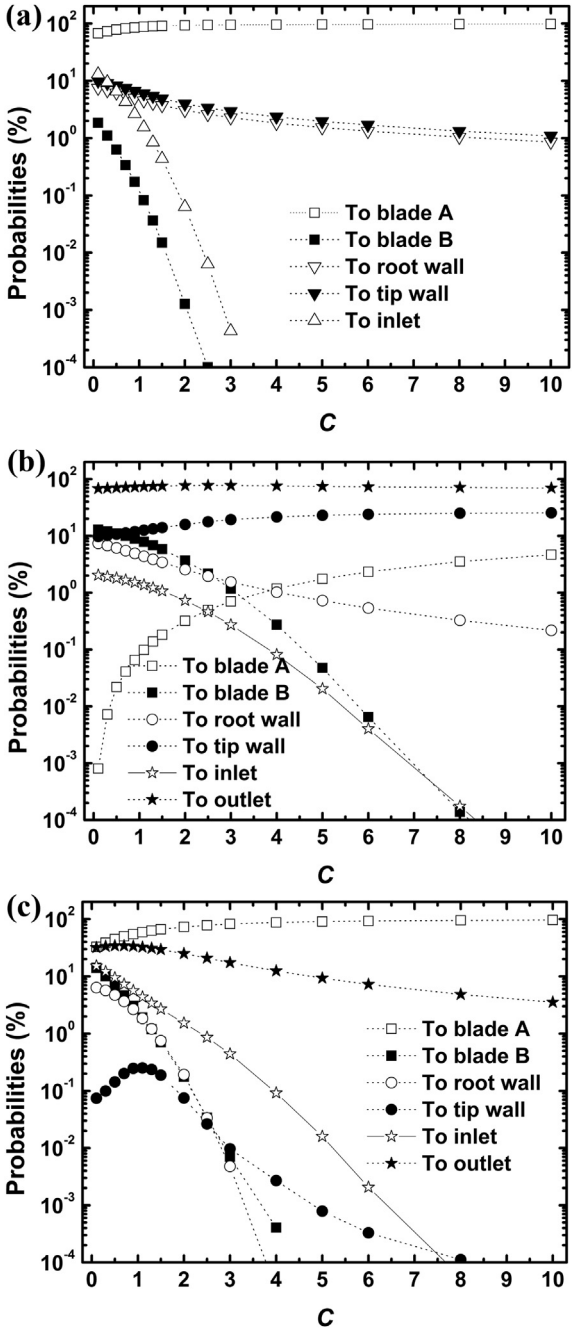

Fig. 4. Probabilities of particles moving from one surface to another versus blade velocity ratio C in a rotor: (a) probabilities of particles moving from the outlet to other surfaces; (b) probabilities of particles moving from blade A to all six surfaces; and (c) probabilities of particles moving from the tip wall to all six surfaces. The results are obtained through TPMC method with the real 3D model. All particles originate from the outlet, and the total number of simulated particles is 1×10^7 for every group of data.

40.59%, respectively, and those of particles moving from the tip wall to blade A and the outlet are 84.40% and 12.87%, respectively. These results illustrate that regardless of whether the particles originate from the inlet or the outlet, the main trajectories of the particles come from blade A to the tip wall, from the tip wall to blade A, or the particles go directly to the outlet. These trends lead to significantly large K_{max} and W.

The molecular trajectories with blade A as the frame of reference and the velocity of the particle along the z axis is assumed to be zero are plotted in Fig. 6. Blade velocity ratio C is 3.0, and the particles leave the midpoint of the center line of either blade A or blade B with velocity $\mathbf{v}$, $\mathbf{v} = 1.0$. The reemission angle changes from $\pi/18$ to $17\pi/18$. Fig. 6 shows that regardless of the reemission angle, most molecules move toward the tip wall. This phenomenon reveals the significant effect of the Coriolis and centrifugal forces. This result is consistent with those shown in Figs. 4 and 5.

A high concentration of particles was observed near the tip wall in cases involving extremely high rotational speed. This location is where the gap between the blades and the tip wall exists. Katsimichas et al. argued that leakage should be a significant factor in such extreme cases. The pumping characteristics of the rotors with clearance δ are presented in Table 1. As mentioned in some books on vacuum, gap length δ could be below 2% of radial blade length h. In Sawada's experiment [3,13], when clearance δ is 0.3 mm and radial blade length h is 18 mm, δ/h is 1.67%. Table 1 shows that when $\delta/h = 1.8\%$, K_{max} increases significantly from 2.474 at $C = 0.5$ to 335.4 at $C = 5.0$. Likewise, W increases from 0.297 at $C = 0.5$ to 0.899 at $C = 5.0$. These results indicate that increasing the rotational speed is an effective method of improving the pumping features of TMPs with clearance. Nevertheless, the conclusion of Katsimichas et al. may still be correct. Comparison of the results of the rotors with $\delta/h = 1.8\%$ and those without clearance shows that K_{max} decreases by 3.74% when $C = 0.5$, 32.50% when $C = 3.0$, and 82.03% when $C = 5.0$. The influence of clearance becomes more significant as C increases.

As shown in Table 1, M_{12} gradually changes as δ increases. The decrease in K_{max} is due mainly to the increase in M_{21}. Parameter

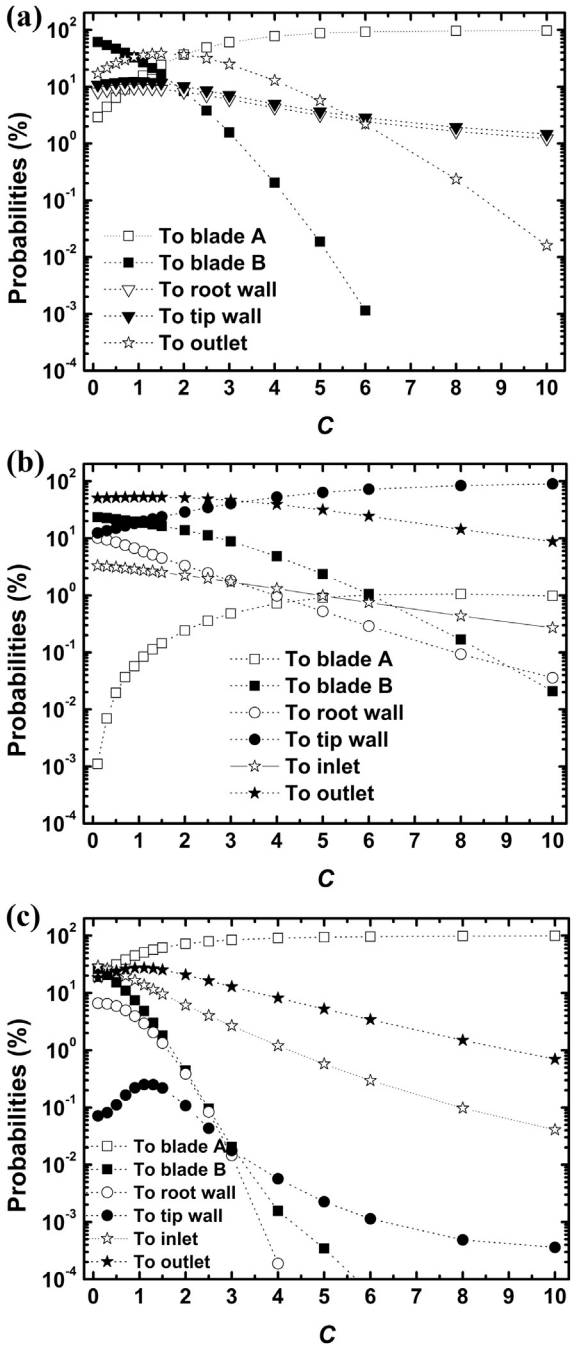

Fig. 5. Probabilities of particles moving from a surface to another surface versus blade velocity ratio C in a rotor: (a) probabilities of particles moving from the inlet to other surfaces; (b) probabilities of particles moving from blade A to all six surfaces; and (c) probabilities of particles moving from the tip wall to all six surfaces. The results are obtained through TPMC method with the real 3D model. All particles originate from the inlet, and the total number of simulated particles is 1×10^7 for every group of data.

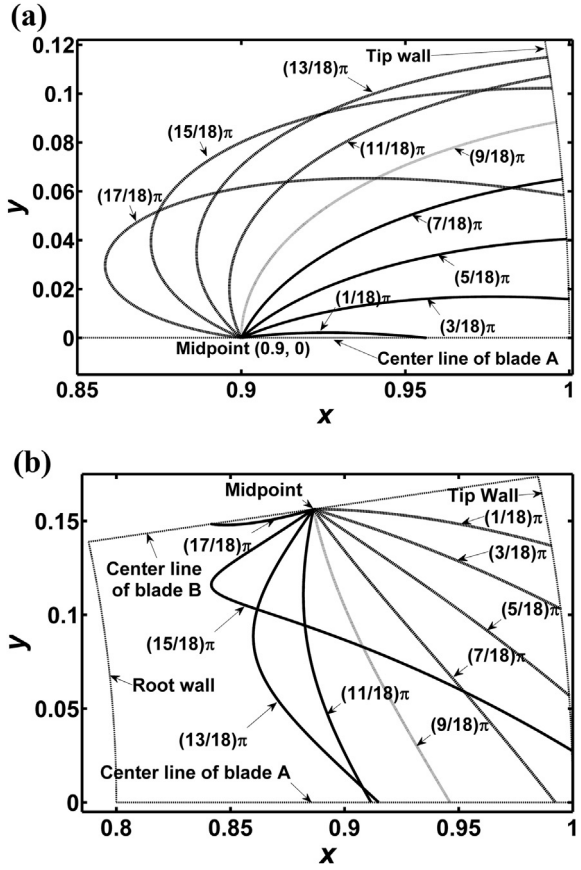

Fig. 6. Particle trajectories in a rotor at $C = 3.0$. Particles leave the midpoint of the center line of either blade A (a) or blade B (b) with velocity $\mathbf{v}$, $\mathbf{v} = 1.0$. The reemission angles of molecules with center lines change from $\pi/18$ to $17\pi/18$; v_z is assumed to be zero.

Table 1
Pumping performance of the rotors with clearance. The results are obtained with a real 3D model through the TPMC method. The number of simulation particles for every value is 10^7.

C	δ/h (%)	M_{12}	M_{21}	m_{out}	K_{max}	W
0.5	0.0	0.49514	0.19265	0.0	2.570	0.3025
	0.6	0.49582	0.19575	0.00139	2.532	0.3001
	1.2	0.49635	0.19821	0.00302	2.504	0.2981
	1.8	0.49768	0.20116	0.00487	2.474	0.2965
	2.5	0.49916	0.20449	0.00731	2.441	0.2947
3	0.0	0.88613	0.01056	0.0	83.92	0.8758
	0.6	0.87854	0.01218	0.00034	72.11	0.8664
	1.2	0.87382	0.01369	0.00090	63.79	0.8601
	1.8	0.86972	0.01535	0.00167	56.65	0.8544
	2.5	0.86582	0.01736	0.00282	49.86	0.8485
5	0.0	0.93469	0.00050	0.0	1866	0.9342
	0.6	0.91723	0.00111	0.00012	825.9	0.9161
	1.2	0.90825	0.00182	0.00045	498.4	0.9064
	1.8	0.90141	0.00269	0.00094	335.4	0.8987
	2.5	0.89435	0.00400	0.00179	223.5	0.8903

m_{out} was defined to evaluate the effect of clearance on M_{21}. If a molecule entering from the outlet is reflected from the tip wall and then moves to the inlet directly with $r > r_{tip}$ or if the molecule moves from the outlet to the inlet directly with $r > r_{tip}$, then such molecule is counted. Simulation of 10^7 particles provided the fraction of counted particles m_{out}. m_{out} is presented in Table 1. Comparison of the results of the rotors with $\delta/h = 2.5\%$ and those without clearance indicates that M_{21} and m_{out} increase by 0.01184 and 0.00731 respectively, when $C = 0.5$; 0.00680 and 0.00282, respectively, when $C = 3.0$; and 0.00350 and 0.00179, respectively, when $C = 5.0$. The increase in m_{out} is almost half of that of M_{21}. In addition, a number of molecules move from outlet to the points near the inlet with $r > r_{tip}$ or may be reflected from the tip wall first and then reach the points near the inlet with $r > r_{tip}$. These molecules still have a high probability of reaching the inlet. All these may be the main leakage trajectories of the particles resulting from the clearance in a rotor. Although m_{out} decreases with the increase in C as a result of the "drag effect" of moving blades introduced by De Simon [21], the values of m_{out}/M_{21} increase significantly as C increases. Thus, a large C would have a significant effect on the pumping performance of a TMP with clearance.

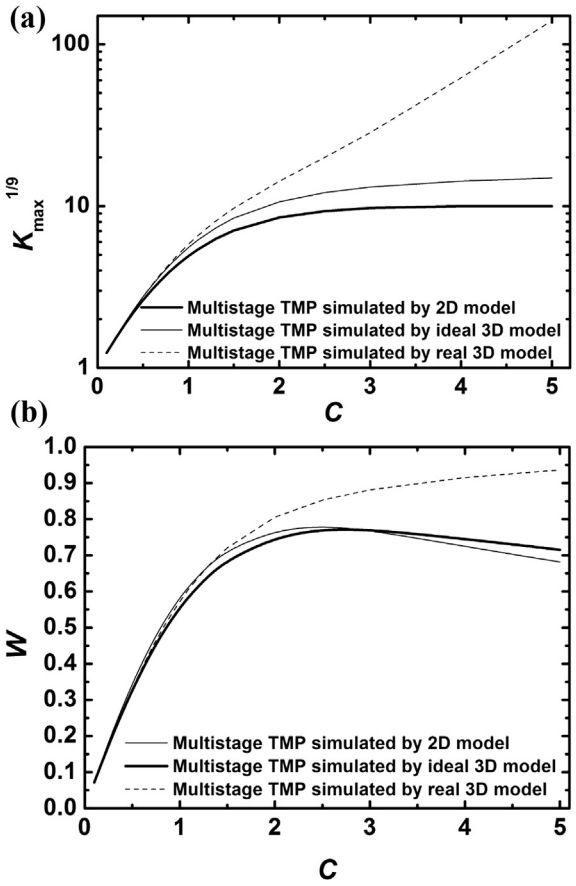

Fig. 7. Pumping performance of the multistage TMP (5 rotors and 4 stators) calculated with the different models: (a) $k_{max}^{1/9}$ versus C and (b) W versus C. The results were obtained with TPMC method, and the number of simulation particles for every value exceeds 5×10^6. A number of suitable weighting factors were used to obtain M_{21}.

3.2. Multistage TMP

The gaps between blades and walls or between successive stages were ignored in the 3D models to simplify the calculation for the multistage TMP. The pumping performance of the multistage TMP (5 rotors and 4 stators) is presented in Fig. 7. The absolute values of relative differences in $K_{max}^{1/9}$ and W between the ideal and real 3D models are less than 0.27% and 1.51%, respectively, in the range of $C \leq 0.5$ and less than 4.50% and 3.17%, respectively, in the range of $C \leq 1.0$. However, the absolute values of relative differences in $K_{max}^{1/9}$ and W between the 2D and real 3D models are less than 4.86% and 4.90%, respectively, in the range of $C \leq 0.5$ and less than 15.4% and 4.90%, respectively, in the range of $C \leq 1.0$. These results indicate that when $C \leq 1.0$, the pumping performance of the TMP is nearly not affected by the Coriolis and centrifugal forces. Given that the moving wall enhances pumping performance and no walls exist in the 2D

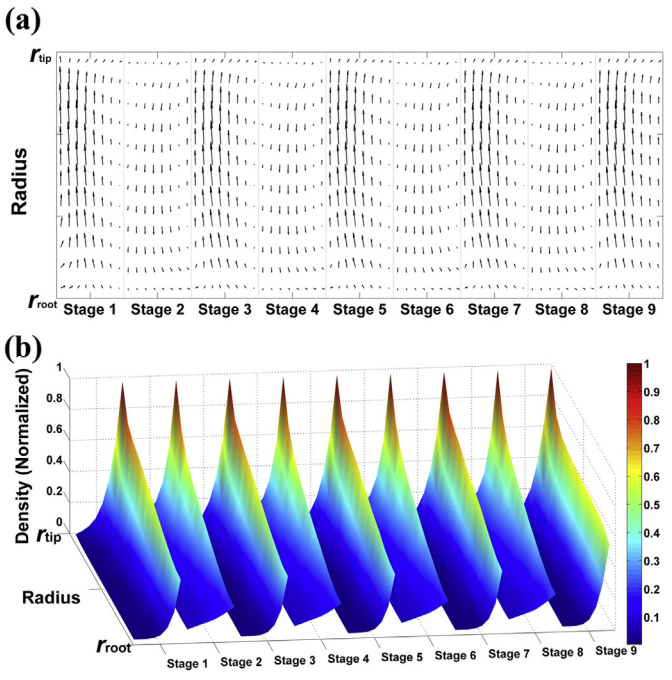

Fig. 8. Flow characteristics and density distribution of gas in the multistage TMP (5 rotors and 4 stators) with zero flow at $C = 3.0$: (a) velocity vectors and (b) density distribution. The density at each point is normalized by the maximum value in each stage. The results were obtained with DSMC method, and the numbers of incident particles per unit time in the inlet and the outlet were determined with TPMC method. The number of total recorded particles in a steady system is 7.6×10^9.

Table 2
K_{max} in each stage of the multistage TMP (5 rotors and 4 stators) at $C = 3.0$. The results were calculated with the DSMC method. The numbers of total statistical particles (sum of N_{out} and N_{in} in each stage) are 2.2×10^9 for the 2D model, 1.4×10^9 for the ideal 3D model, and 2.4×10^8 for the real 3D model.

Number of stages	1	2	3	4	5	6	7	8	9
2D model	10.15	9.696	9.716	9.721	9.718	9.721	9.710	9.710	9.419
Ideal 3D model	13.51	12.96	12.98	12.97	12.99	12.98	12.99	13.01	13.60
Real 3D model	86.75	7.178	86.37	7.205	86.63	7.101	86.08	7.097	84.66

model, the ideal 3D model is a more suitable substitute for the real 3D model than the 2D model. Fig. 7 also indicates that the $K_{max}^{1/9}$ of the multistage TMP calculated with the 2D or ideal 3D model saturates with the increase in C; however, those calculated with the real 3D models increase exponentially. W of the multistage TMP calculated with the real 3D model increases to almost 1.0, and those calculated with the 2D and ideal 3D models reach their maximum at $C = 2.5$. These results are consistent with those obtained with single-stage TMP.

Fig. 8 shows the flow characteristics and density distribution (normalized by the maximum value in each stage) of gas in the multistage TMP with zero flow at $C = 3.0$. The images of velocity vectors in each rotor or stator are similar as seen in Fig. 8(a). The molecules in a rotor move toward the tip wall, whereas those in a stator diffuse in the opposite direction. Fig. 8(b) shows that molecules gather near the tip wall; the maximum normalized gas density near the root wall in a stator is lower than that in a rotor. This trend is consistent with the gas flow shown in Fig. 8(a). Fig. 8(b) also shows that except for stage 9, only slight differences exist in normalized gas density distribution in the different rotors or stators. The gas flow and density distribution features in a single-stage TMP are similar to those in the last stage of the multistage TMP because the gas primarily comes from the downstream side in both single-stage and multistage TMPs; thus, these parameters are not presented in this study.

Table 2 presents the K_{max} in each stage of the multistage TMP at $C = 3.0$. Given that the velocity spectrum of molecules between two successive stages does not obey the Maxwellian distribution, the K_{max} of each stage is defined as N_{out}/N_{in}, where N_{out} and N_{in} are the total numbers of molecules passing through the outlet and the inlet per unit time, respectively. Only slight differences were observed between the results of the rotors and stators for the 2D or ideal 3D model but not for the real 3D model. The K_{max} in each stage simulated by the 2D model is in the range of 9.419–10.15, which is close to the result of a single-stage TMP (9.84 at $C = 3.0$). The K_{max} in each stage simulated by the ideal 3D model is in the range of 12.96–13.60, which is slightly lower than the result of a single-stage TMP (14.20 at $C = 3.0$). However, the K_{max} simulated by the real 3D model ranges from 84.66 to 86.75 for the rotors and from 7.097 to 7.205 for the stators. The values of the stators are significantly lower than that of a single stator (84.01 for the rotor and 13.12 for the stator at $C = 3.0$).

As reported by Tu et al. [2,12], a number of molecules would pass directly through the blade channel without colliding with either blades in a 2D model. The blade velocity of the adjacent stage relative to these molecules may be equal to zero. Thus, these molecules should be analyzed separately. In a real 3D model, molecules that collide with the tip wall and then enter an adjacent stator or those that collide with the root wall before entering an adjacent rotor should also be considered. According to the theory of Tu et al., the correct transmission probability in each stage is as follows:

$$\begin{aligned} M_{12}^c(j) &= M_{12}(1-P_j) + M_{12}^0 P_j \\ M_{12}^c(j) &= M_{21}(1-Q_j) + M_{21}^0 Q_j \end{aligned} \quad (5)$$

where $M^c(j)$ is the correct transmission probability of stage j; M and M^0 indicate the transmission probabilities of the single-stage TMP at $C = 3.0$ and 0.0, respectively; and P and Q are the correction factors for the transmission probabilities in the forward and backward directions, respectively. P and Q are the fractions of the incident molecules in stage j per unit time whose stream velocity relative to stage j is 0, they were obtained through the DSMC method, and the K_{max} in each stage was obtained with Eqs. (3) and (5). The K_{max} of the stators ranges from 7.52 to 8.67 in a real 3D model and is close to the results shown in Table 2. A large K_{max} is often obtained with a small Q. In this study, Q_9 is 0; the other values of Q are less than 5.3×10^{-5} for the 2D model, from 0.025 to 0.072 for the ideal 3D model, and from 0.121 to 0.179 for the real 3D model. Tip and root walls do not exist in the 2D model; thus, this model has the lowest Q and the K_{max} in each stage is close to that of the single-stage TMP. The molecules exhibit centrifugal motions when the real 3D model is used; thus, the real 3D stators have the largest Q and their K_{max} is significantly lower than that of the single stator. Actually, the velocity spectra of incident molecules that deviate from a Maxwellian distribution lead to a relatively different result [11]. Although the theory of Tu et al. cannot accurately describe the pumping features of a TMP, a qualitative analysis based on their theory is still beneficial. Nowadays, a TMP with extremely high rotational speed may be impractical and uneconomical. However, with the development of magnetic suspension-type TMPs [25,26], a special TMP may be designed for special purposes, such as spacecraft usage [27] or other important industrial and scientific applications.

4. Conclusions

Selecting a suitable model is a key factor for the quick and accurate calculation of the pumping performance of TMPs. In this study, three different models were investigated in the free molecular flow range. Accurate numerical results were obtained by the ideal 3D model, which is nearly as simple as the 2D model, when $C \leq 1.0$. The centrifugal motion of molecules in a real 3D rotor resulted in a significantly large compression ratio and perfect pumping speed when $C \geq 2.0$. Given the same conditions, the 2D and ideal 3D models provided a massive underestimate of pumping performance. In addition, the results also show that the K_{max} of a stator is much lower than that of a rotor in the real 3D model when $C \geq 2.0$.

References

[1] Kruger CH. Ph.D. thesis. Department of Mechanical Engineering, MIT: Cambridge, MA; 1960.
[2] Tu JY, Yang NH. Vacuum 1987;37:831.
[3] Sawada T. Bull JSME 1979;22:362.
[4] Katsimichas S, Goddard AJH, Lewington R, de Oliveira CRE. J Vac Sci Technol A 1995;13:2954.
[5] Chu JG, Hua ZY. J Vac Sci Technol 1982;20:1101.
[6] Sharipov F. J Vac Sci Technol A 2010;28:1312.
[7] Bird GA. J Vac Sci Technol A 2011;29:011016.
[8] Sengil N. Vacuum 2012;86:1764.
[9] Sengil N, Edis FO. Comput Fluids 2011;45:202.
[10] Heo JS, Hwang YK. Vacuum 2000;56:133.
[11] Schneider TN, Katsimichas S, de Oliveira CRE, Goddard AJH. Vacuum 1997;48:449.

[12] Tu JY, Yang NH, Pang SJ, Zu Y. J Vac Sci Technol A 1988;6:2535.
[13] Versluis R, Dorsman R, Thielen L, Roos ME. J Vac Sci Technol A 2009;27:543.
[14] Chang YW, Jou RY. Appl Surf Sci 2001;169–170:772.
[15] Wang S, Ninokata H, Merzari E, Lei K, Luo X, Lu L, et al. Vacuum 2009;83:1106.
[16] Wang S, Ninokata H. Prog Nucl Energy 2005;47:664.
[17] Amoli A, Ebrahimi R, Hosseinalipour SM. Vacuum 2004;72:427.
[18] Amoli A, Hoseinalipour M, Ebrahimi R. AIAA Paper 2003-3777.
[19] Hosseinalipour SM, Amoli A, Ebrahimi R. J Thermophys Heat Transf 2004;18:148.
[20] Shams M, Sheykhzadeh H, Taghavi M. J Disper Sci Technol 2010;31:299.
[21] De Simon M. Vacuum 1990;41:2021.
[22] Bird GA. Molecular gas dynamics and the direct simulation of gas flows. Oxford: Clarendon Press; 1994.
[23] Varoutis S, Valougeorgis D, Sharipov F. J Vac Sci Technol A 2009;27:1377.
[24] Sharipov F. Vacuum 2013;90:25.
[25] Kabelitz HP, Fremerey JK. Vacuum 1988;38:673.
[26] Ishizawa T, Miki M, Urano C, Kawashima T, Yamamoto M, Masubuchi N. J Vac Sci Technol A 1987;5:2965.
[27] Henning J. Vacuum 1979;29:447.